Impact of CeO_2 substitution on structural, magnetic and ferroelectric properties Of $BiFeO_3$-$BaTiO_3$ lead free multiferroics for actuator applications

I. R. Budumuru [a], K. V. Ramesh [a,*], M. N. V. Ramesh [a], D. Venkatesh [b], T. D. Rao [a]

[a] *Department of Physics, GITAM School of Science, GITAM Deemed to be University, Rushikonda, Visakhapatnam, Andhra Pradesh- 530045, India*

[b] *Department of Physics, B V Raju Institute of Technology, Narsapur, Medak, Telangana- 502313, India*

Ce-doped polycrystalline $0.7BiFeO_3$-$0.3(BaTi_{1-x}Ce_xO_3)$ (x=0.00-0.07) ceramics were synthesized via solid-state method. XRD confirmed a rhombohedral perovskite structure, with lattice parameters and Fe-O bonds showing distortions upon Ce addition. FE-SEM revealed homogeneous grain distribution with well-defined boundaries, indicating densification. Magnetic measurements using VSM showed variations in the saturation magnetization and coercivity with Ce ions. The highest magnetization occurred at x=0.03 and decreased at higher concentrations due to Fe^{3+} superexchange interaction dilution. Dielectric measurements showed Curie temperature decreased and then stabilized at higher Ce concentrations. Polarization-electric field loops indicated a transition from ferroelectric to relaxor behavior, with the Ce concentration improving energy recovery for storage applications.

(Received August 23, 2025; Accepted November 20, 2025)

Keywords: Solid state reaction, Multiferroic, $BiFeO_3$-$BaTiO_3$, VSM, P-E loop

1. Introduction

Multiferroic materials have become an important research area in materials science. These materials exhibit several ferroic properties, such as ferroelectricity, ferromagnetism, and ferroelasticity. Multiferroics are appealing because of their potential applications in energy-harvesting systems, sensing devices, and data storage. The magnetoelectric (ME) effect, which allows the magnetic characteristics to be controlled by electric forces or vice versa, is a particularly intriguing feature of multiferroics [1]. The development of novel devices with dual functionality is facilitated by this coupling mechanism, which is frequently ascribed to the Dzyaloshinskii-Moriya interaction [2]. However, identifying materials that exhibit strong magnetoelectric coupling at room temperature is the main challenge in multiferroic research. For practical applications, single-phase multiferroics must be enhanced because they typically exhibit weak interactions.

Bismuth ferrite, often known as $BiFeO_3$ or BFO, is a multiferroic material that has attracted considerable interest due to its exceptional capacity to display both ferroelectric and antiferromagnetic characteristics at normal temperature [3-4]. Its structure is a deformed rhombohedral perovskite with alternating layers of Bi and Fe ions in the R3c space group [5]. This configuration permits antiferromagnetism through superexchange interactions between Fe^{3+} ions and ferroelectricity through the Bi^{3+} lone pair stereochemical activity [6]. BFO can operate in a variety of settings due to its high Curie temperature (T_c) of approximately 1083-1143K and Néel temperature (T_N) of approximately 595-667K [7-8]. However, their structural instability, large leakage currents, and poor magnetoelectric coupling limit their practical applications. When ABO_3 perovskites form a composite with $BiFeO_3$, it helps stabilize the crystal structure and improve the electrical properties.[9]. $BiFeO_3$ - $BaTiO_3$ lead-free piezoceramics have been studied to optimize their ferroelectric and piezoelectric performance [10-12]. To overcome these challenges, various researchers have investigated composite systems combining BFO with other ABO_3 perovskites, such

* Corresponding author: kvramesh11@gmail.com
https://doi.org/10.15251/JOR.2025.216.769

as $BaTiO_3$ (BT) [13]. The enhanced stability of the perovskite structure and the decrease in oxygen vacancies help explain the better electric characteristics of the $0.7BiFeO_3$-$0.3BaTiO_3$ (0.7BF-0.3BT) composite. The 0.7BF-0.3BT system has been reported to have excellent piezoelectric properties with d_{33} = 210 pC/N, high T_c = 507 °C, and low leakage current density, making it suitable for high-temperature applications [12].

Doping with rare-earth elements, including Sm^{3+}, La^{3+}, Nd^{3+}, Yb^{3+}, Er^{3+}, Gd^{3+}, and Ce^{3+}, is a crucial approach for improving the properties of BFO and its composites [9, 14-17]. These elements produce oxygen vacancies when doped at A or B-sites of the perovskite lattice, thereby improving ferromagnetic interactions and simultaneously lowering leakage currents. For example, lattice strain induced by Ce^{3+} doping not only stabilizes the rhombohedral phase, but also increases polarization and magnetization, thus producing multifarious behavior [8]. Apart from structural enhancements, rare-earth doping improves the dielectric constant, ferroelectric switching, and energy-storage capacity. For instance, Ce doping in the BFO-BT system has been demonstrated to significantly increase the dielectric constant and lower dielectric losses, thereby qualifying these materials for high-frequency applications [6]. Moreover, the reduction of antiferromagnetic spin cycloids by doping improves magnetoelectric coupling, thereby providing new opportunities for sensor and actuator technologies [18]. In this study, rare earth cerium (Ce) was doped into the Ti sites of $BaTiO_3$ in the 0.7BF–0.3BT composite to further enhance the properties of 0.7BF-0.3BT. also deeper understanding of the influence of Ce addition on the structural, ferromagnetic, and electric properties of the 0.7BF–0.3BT system by systematically varying the Ce concentrations and studying their effects to determine the optimal doping level for enhancing the material properties of the system for data storage, energy harvesting, and sensing applications.

2. Experimental

$0.7BiFeO_3 – 0.3(BaTi_{1-x}Ce_xO_3)$ ceramics (x=0,0.01,0.03,0.05 and 0.07 abbreviated as Ce00, Ce01, Ce03, Ce05 and Ce07 respectively) were synthesized by using the conventional solid-state reaction method. Analytical grade Bi_2O_3, Fe_2O_3, BaO, CeO_2, and TiO_2 powders were used. All the powders were weighed in stoichiometric proportions and mixed thoroughly. In addition, 10 mol% Bi_2O_3 was used in addition to the required proportion to compensate for evaporation loss during sintering. The resultant mixture for 4h in an agate mortar for homogeneity. The mixture was then transferred into a crucible and calcined in an oven at 800°C in a furnace for 2h. The samples were pressed into pellets in a 10 mm die using a hydraulic press at the optimum pressure. The pellets were sintered at 800°C at 2 hours in a furnace. The sintering of the samples was controlled to minimize defects, such as secondary phases and porosity, which influence the dielectric and ferroelectric properties. The densities of all the samples were determined using the Archimedes principle. For electrical property analysis, silver paste was applied on both sides of the pellets and heated at 500°C for one hour.

Crystallographic analysis of all samples was performed using an X-ray diffractometer (Bruker Advanced with Cu Kα 1.5406 Å) for the structural and phase identification of the samples. Surface morphology and elemental identification of the samples were carried out using FESEM (TESCAN-MIRA) with an accelerating voltage of 25 keV. The magnetic measurements were performed using a vibrating sample magnetometer (Lakeshore VSM 7410). The dielectric properties of all samples were measured using an impedance analyzer (PSM 1735 Newton 4th Ltd) from room temperature to 500 °C at a frequency of 1 MHz. P-E loop analysis of the samples was performed using a P-E loop tracer of Radiant Technologies.

3. Results and discussion

3.1. Structural studies

The X-ray diffraction (XRD) patterns of $0.7BiFeO_3$ - $0.3(BaTi_{1-x}Ce_xO_3)$, with x=0.00, 0.01, 0.03, 0.05, and 0.07 samples, are shown in Fig. 1. The Rietveld analysis shown in Fig. 1 confirmed that all samples exhibited a rhombohedral perovskite structure belonging to the R3c space group.

This is in line with existing literature [8]. The values obtained from XRD refinement are presented in Table 1. The most intense diffraction peak was observed at approximately 31.85°, as shown in Fig. 2, indicating a rhombohedral perovskite structure of the samples. The lower angle side diffraction peak shift indicates the lattice expansion of the present samples. Furthermore, some small diffraction peaks observed at approximately 30°are probably related to the secondary phases generated during sample processing. These peaks imply the presence of localized structural distortions resulting from Ce ion addition, even though they have no appreciable effect on the structural integrity of the main rhombohedral phase [19]. From the refinement data, Ce addition causes a variation in the lattice constant and increases the volume of unit-cell, which is due to the difference in ionic radii between Ce (1.01 Å) and Ti (0.67 Å) ions. which results in lattice distortions due to the differences in the ionic radii. Similar kinds of lattice distortions were also observed for various rare earth elements doped $BiFeO_3$ due to the larger ionic radii of rare-earth elements leading to increased unit cell volume [20-21].

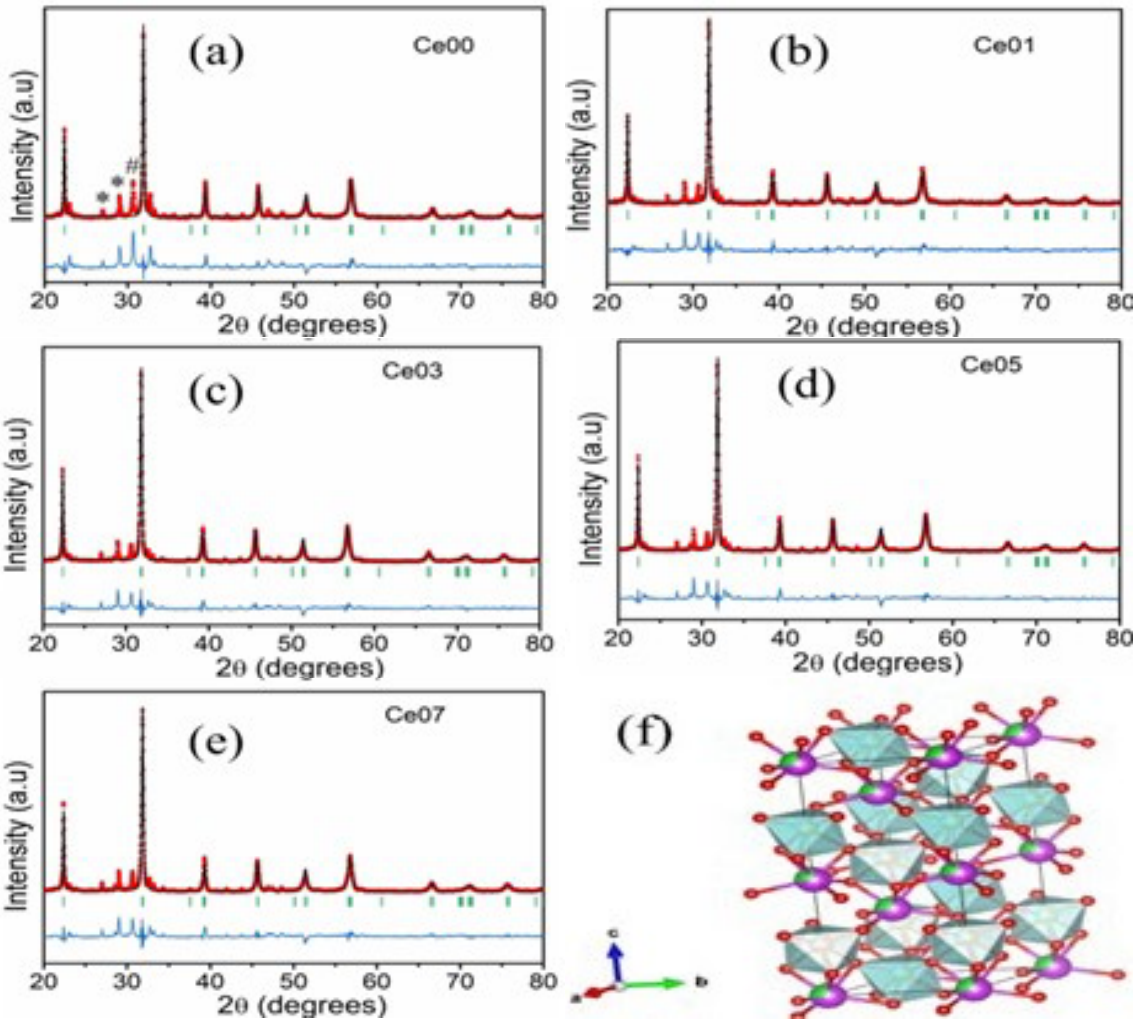

Fig. 1. Reitveld XRD diffractograms of $0.7BiFeO_3$ - $0.3(BaTi_{1-x}Ce_xO_3)$ (a-e: x=0.00 to 0.07) and (f) Crystal structure.

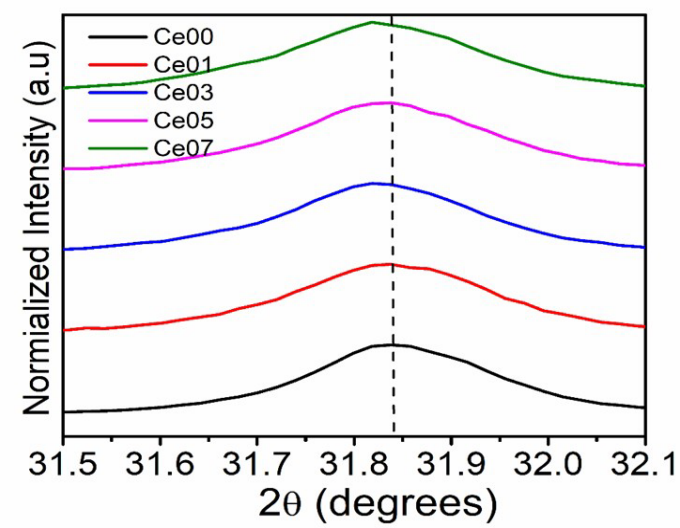

Fig. 2. Magnified view of the peak near 31.85 for 0≤ x≤0.07.

Table 1. Lattice parameters of $0.7BiFeO_3$ - $0.3(BaTi_{1-x}Ce_xO_3)$ ceramics [x=0,0.01,0.03,0.05,0.07]. The numbers in parentheses denote the uncertainty in the least significant digit.

Parameter	**Ce00**	**Ce01**	**Ce03**	**Ce05**	**Ce07**
a Å	5.6067(19)	5.6099(9)	5.6114(7)	5.6100(7)	5.6093(8)
c Å	13.770(6)	13.798(3)	13.799(2)	13.796(2)	13.803(2)
V $Å^3$	374.8687	376.0598	376.2883	376.0188	376.1157
Fe-O-Fe	154(4)	151.3(15)	157.0(15)	155.7(15)	157.5(15)
Fe-O1	2.12(11)	2.18(4)	2.10(4)	2.07(4)	2.06(4)
Fe-O2	1.95(11)	1.92(4)	1.96(4)	1.99(4)	1.99(4)
<Fe-O>	8.01	4.54	9.18	8.91	9

Additionally, the influence of Ce^{3+} ions in the $0.7BiFeO_3$-$0.3(BaTi_{1-x}Ce_xO_3)$ system was studied using the Fe-O bond angles and bond lengths calculated by XRD Rietveld refinement analysis; the obtained values are given in Table 1. Fe-O-Fe bond angle measurements play a significant role in understanding the magnetic properties of materials. In the present investigation, the Fe-O-Fe bond angle was observed for Ce0 (154°) and varied with the Ce concentration from Ce01(151.3°) to Ce07(157.5°). This type of nonlinear variation in the Fe-O-Fe bond angles with the addition of Ce^{3+} initially at lower concentrations distorts the octahedral sites and is structurally stabilized at higher concentrations. The enhanced Fe-O-Fe bond angles at higher concentrations reduced the B-site tilting and improved the Fe^{3+}–O^{2-}-Fe^{3+} magnetic super-exchange interactions. The variations in the Fe-O1 bond lengths also confirm the influence of Ce on the perovskite lattice. Initially, it increased for the Ce01 sample, indicating lattice expansion; for the remaining concentrations, the Fe-O1 bond lengths decreased, suggesting contraction of the B-site, which resulted in lattice strain. The Fe-O2 bond length has very low fluctuations, indicating major structural changes along the Fe-O1 axis. The average Fe-O bond length varied with the Ce^{3+} concentration and reached a maximum for the Ce03 sample (Å) and stabilized for the Ce05 and Ce07 samples. This behavior indicates that most structural modifications occurred in the Ce03 sample, creating an ideal equilibrium between the lattice expansion, polarization retention, and minimized B-site distortion. The broadening of the small peaks with the addition of Ce^{3+} ions suggests that the prepared samples have particle sizes in the nano range, as confirmed by Field

Emission scanning electron microscopy (FESEM) analysis. The three-dimensional crystal structure of the $0.7BiFeO_3$-$0.3(BaTi_{1-x}Ce_xO_3)$ system was drawn with the help of VESTA 3 software [22], and it is shown in Fig. 1(f).

3.2. Morphological studies

The FESEM images of the Ce00, Ce01, Ce03, Ce05, and Ce07 samples are shown in Fig. 3. All FESEM images were taken at 60k magnification and 500 nm resolution.

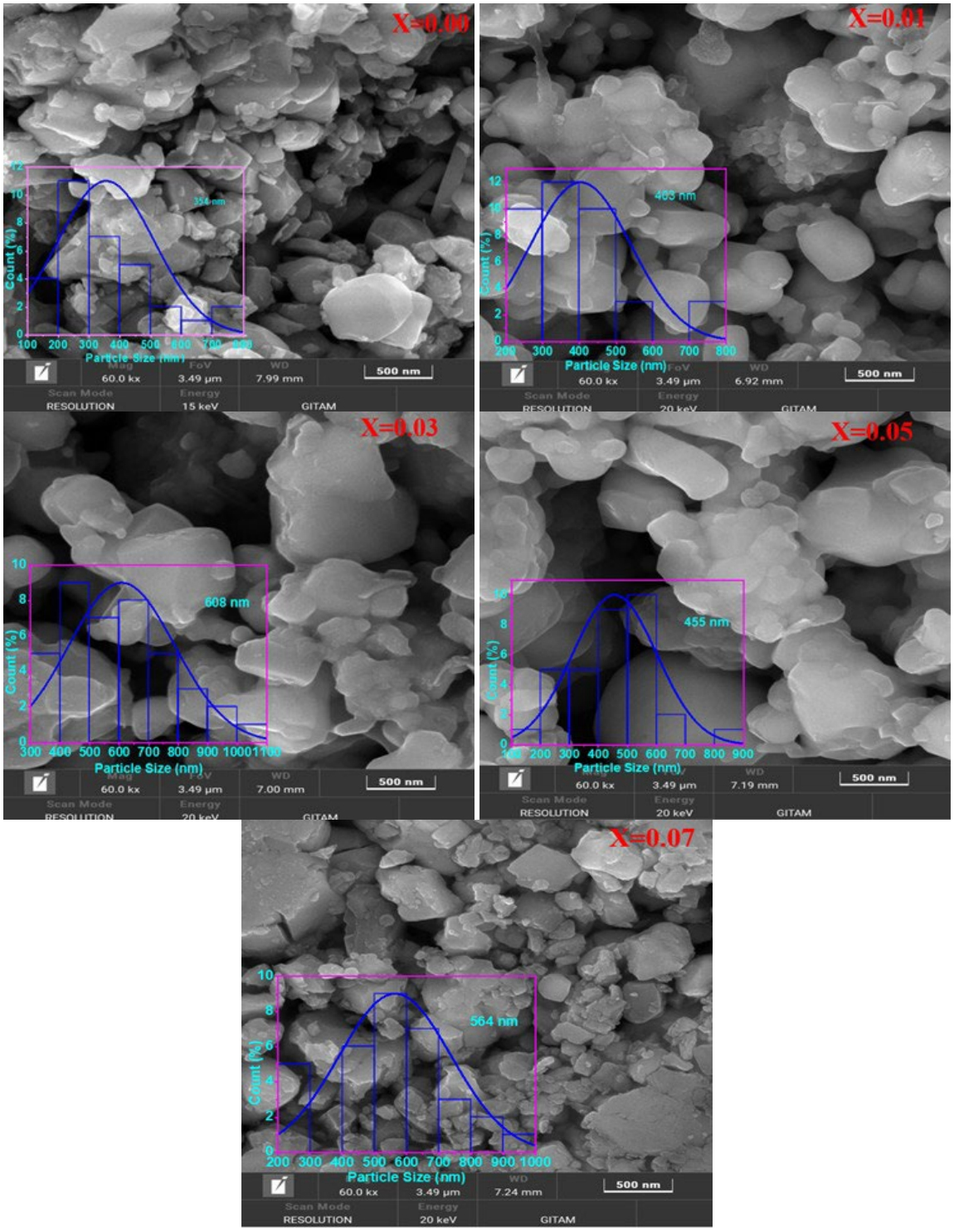

Fig. 3. SEM of micrographs on polished and thermally etched surfaces of $0.7BiFeO_3$ - $0.3(BaTi_{1-x}Ce_xO_3)$ ceramics: (a) x=0, (b) x=0.01, (c) x=0.03, (d) x=0.05, (e) x=0.07.

The FESEM images revealed a homogeneous distribution of well-defined grains of varying sizes with clear grain boundaries. In addition, the microstructure of the sample clearly indicated that the surface was densely populated with grains. The sintered samples exhibited a layered compound structure, which aligns with previous reports [20, 23]. The average grain size of the samples was in the range of 354-608 nm. The larger grain size and better grain boundaries of the samples indicate the highly dense and polycrystalline nature of the material. The nature of the samples plays an important role in improving their magnetic and electrical properties.

3.3. Magnetic studies

The magnetic behavior of the Ce00, Ce01, Ce03, Ce05, and Ce07 samples are shown in Fig. 4. From the VSM graphs, magnetic properties such as saturation magnetization (Ms), remanent magnetization (Mr), and coercivity (Hc) of the samples were calculated, and the obtained values are listed in Table 2.

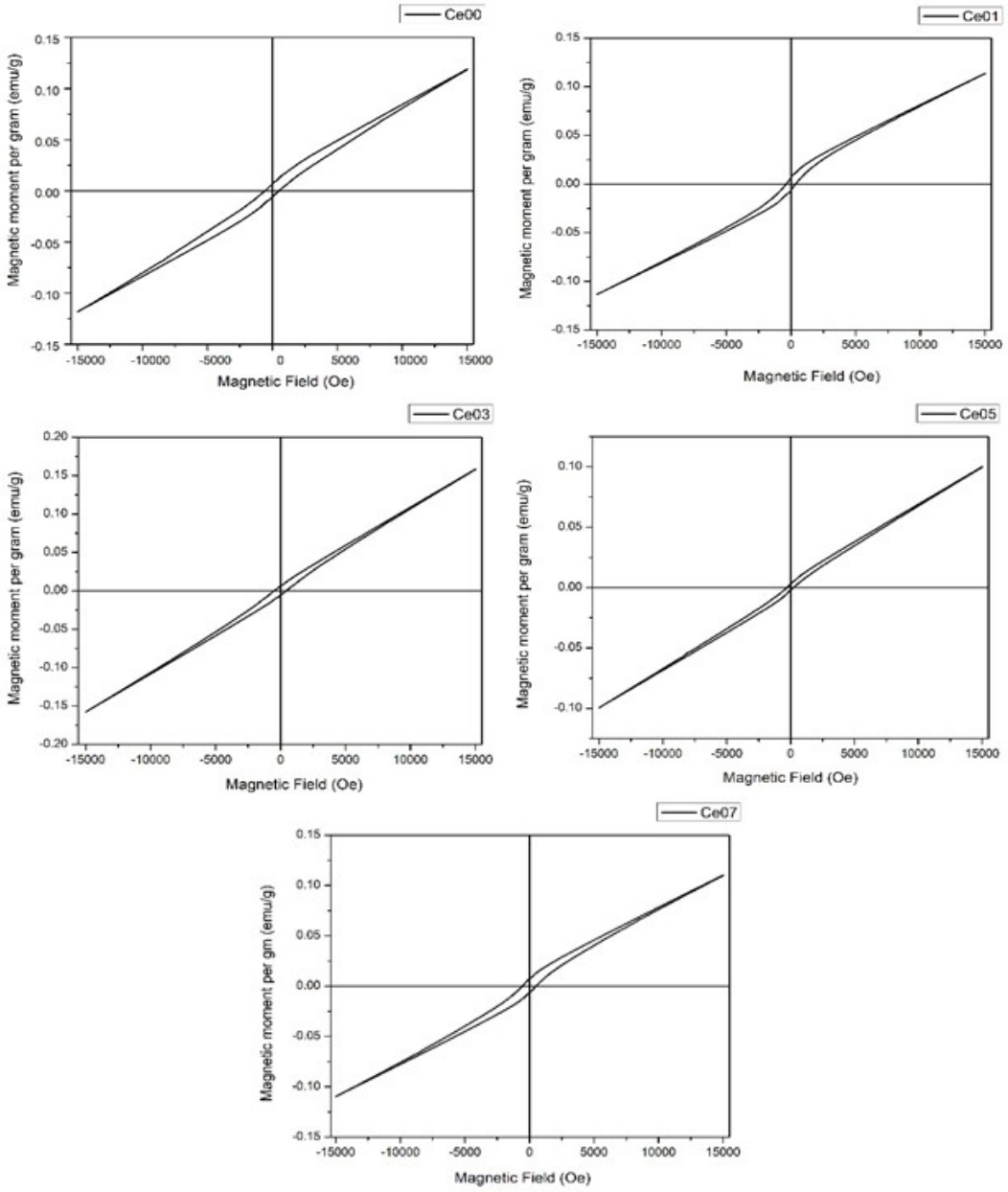

Fig. 4. Magnetic hysteresis loops of $0.7BiFeO_3$ - $0.3(BaTi_{1-x}Ce_xO_3)$ ceramics [x=0,0.01,0.03,0.05,0.07].

Table 2. Parameters from Magnetic hysteresis loops of $0.7BiFeO_3$-$0.3(BaTi_{1-x}Ce_xO_3)$ ceramics [x=0,0.01,0.03,0.05,0.07].

Sample	Saturation magnetization M_s (emu/g)	Remanent Magnetization M_r (emu/g)	Coercive field H_c (Oe)	Magnetic anisotropy (K)
Ce00	0.119	59.32	557.7	69.2
Ce01	0.114	58.86	258.2	30.6
Ce03	0.158	53.31	552.0	91.1
Ce05	0.100	78.71	278.2	28.9
Ce07	0.110	64.05	557.6	64.0

The variations in the Ms, remanence, and coercivity are directly related to the variations in the lattice parameters, Fe-O-Fe bond lengths, and angles. From the XRD studies, it is also clear that these structural variations affect the magnetic super-exchange interactions of the A and B sites. The addition of Ce ions influenced the magnetic properties, the basic sample Ce00 exhibited a mild saturation magnetization (0.1191 emu/g). In addition, the magnetization initially decreased in Ce01 (0.1136 emu/g) and increased in Ce03 (0.1584 emu/g). The significant improvement in Ms for the Ce03 sample suggests that Ce addition disturbed the spin configuration of $BiFeO_3$, resulting in an enhanced net magnetic moment of the sample. In addition, it aligns with the XRD data showing an ideal increase in the unit cell volume and slight structural changes in this sample. These variations align with those of other rare-earth-substituted $BiFeO_3$–$BaTiO_3$ ceramics from existing reports [24]. At higher Ce concentrations Ce05 and Ce07 sample the magnetization is decreased in which is due of the non-magnetic nature of the Ce ions. The coercivity values exhibited a nonlinear trend with the composition. Initially, it decreased from 557.67 Oe to 258.21 Oe for the Ce01 sample and increased for the Ce03 and Ce07 samples. The initial decrease indicates that Ce addition has fewer pinning effects on the domain walls, enabling magnetization reversal. The increase in Hc indicates that Ce addition enhances magnetic anisotropy, which improves the energy required to invert the magnetic domains. This behavior corresponds to previous studies on Ce-doped magnetite, where the initial decrease in coercivity was due to improved domain wall mobility linked to lattice distortions and anisotropic interactions [25]. The remanence Mr exhibited significant variations with the Ce ion concentration. The maximum remanence observed for the Ce05 sample suggests improved alignment of the magnetic domains and reduced spin canting, resulting in stronger ferromagnetic behavior. The magnetic crystallographic anisotropy of the samples was calculated using the standard formula K=(Ms*Hc)/0.96, where Hc-coercivity and Ms-saturation magnetization. The obtained magnetic anisotropy values are listed in Table 2. The high K value observed for the Ce03 sample indicates that the addition of Ce maximizes anisotropic interactions. At higher concentrations of Ce05 and Ce07, the K values decreased due to increased lattice distortions and weak exchange interactions in the sample. The changes in the magnetic properties with Ce ion addition alter the domain structure and spin-orbit coupling, making these materials suitable for multiferroic and spintronic applications.

3.4. Dielectric studies

Fig. 5 shows the variation in the dielectric properties of the Ce-doped BFO-BT ceramics at a frequency of 1 MHz. The maximum peak temperature (Curie temperature, Tc) first decreased with Ce doping, and thereafter, Tc remained constant or unaffected by Ce doping. Generally, Ce exists in two oxidation states, Ce^{3+} and Ce^{4+}. When Ce is doped into $BaTiO_3$, it can enter the A or B-site depending on the Ba/Ti ratio and sintering conditions [26-27]. At low Ce doping values (< 8 at%), it can enter the A-site of the ABO_3 perovskite.

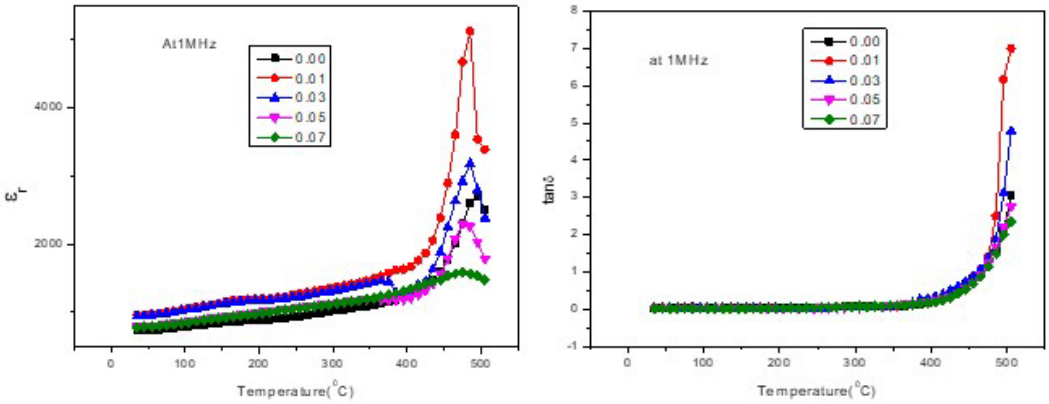

Fig. 5. Dielectric studies of $0.7BiFeO_3$ - $0.3(BaTi_{1-x}Ce_xO_3)$ ceramics [x=0,0.01,0.03,0.05,0.07].

Here, ionic radii of Ce (Ce^{3+}1.34 A.U and for Ce^{4+} 0.87 A.U for 12 & 6 coordination no.s respectively), Ba^{2+} (1.61 A.U for 12 CN), and Ti^{4+} (0.601 for 6 CN) are close to Ba^{2+} and Ti^{4+}. Therefore, it can enter either the Ba^{2+} or Ti^{4+} sites. In the present study, it may have entered the A-site. The reasons for this are as follows. Fig. 5 shows almost no effect on the Curie temperature when Ce was doped into the material. Min Shang et al. [28] showed that, in the case of BCZT, the Curie temperature was unaffected by A-site doping compared to B-site doping. It has been shown that the mismatch in the ionic radii of different ions generates a local strain field called the "σ^2" effect. This is the local electric field generated by the chemical valence mismatch between the host and dopant ions [29]. In the present study, the A-site was occupied by Ba, Bi, and Fe ions. Simultaneously, chemical valence mismatch situations may be compensated by other compensation mechanisms, such as titanium valence compensation [30]. Wei Li et al [31] studied Ce doping into 0.67BF-0.33BT and observed that the Curie temperature was unaffected up to a certain amount of Ce doping into the Bi^{3+} site. In the present study, Tc is nearly constant at higher Ce concentrations Ce005, and Ce007 indicates that the effects of the strain fields are largely offset by alternative mechanisms, such as charge balancing through shifts in Ti valence. Fig. 5 shows the variation in tan δ with temperature. The dielectric loss is nearly independent of the temperature over a temperature range and increases at high temperatures. This behavior is due to temperature-dependent conduction processes, such as the movement of oxygen ions at higher temperatures. The stable dielectric response of the present Ce-doped BFO-BT system indicates that the defect dipoles have a limited impact on the polarization mechanism.

3.5. P-E loop studies

The ferroelectric properties of the Ce-doped BFO-BT ceramics were calculated using a polarization–electric field (P-E loop) graph, as shown in Fig. 6. The values of Ec and Pr obtained for the samples are listed in Table 3. The remanence and coercivity decreased with increasing Ce concentration. As shown in Fig. 6, as the Ce concentration increased, the P-E loop narrowed, indicating the relaxor behavior of the samples [30]. This type of transition is typically observed in the $BiFeO_3$-based ceramics. Ec decreased from 1673.2 kV/cm^3 (Ce00) to 738 kV/cm^3 (Ce007), and Pr also followed the same trend, decreasing from 0.03 (Ce00) to 0.0092 μC/cm^2. The observed decrease in Ec indicates improved domain wall mobility with increasing Ce concentration. This also suggests a shift from typical ferroelectric behavior towards a more disordered relaxor state. This relaxor behavior was due to the addition of Ce ions, which introduced lattice distortions in the samples, as observed in the XRD studies. These strain fields create localized electric fields that interfere with the long-range ferroelectric order and promote diffuse phase transition, which is evident from the narrow P-E loops of the sample. The decrease in Pr indicates weakening of the ferroelectric domain alignment. The energy storage density (Wrec), of all samples was calculated using the standard relation [32], and the obtained values are listed in Table 3. Wrec increased with increasing Ce concentration, and the maximum value was observed for the Ce07 sample, which was

due to an increase in Es and decrease in Pr. The obtained results confirmed that these Ce-doped BF-BT ceramics are suitable for energy storage applications.

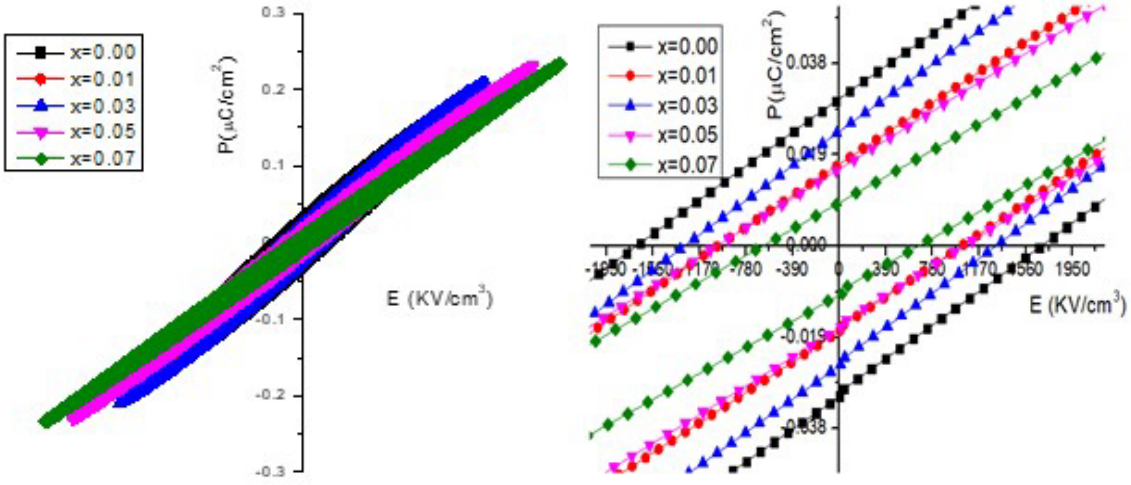

Fig. 6. P-E hysteresis loops of $0.7BiFeO_3$- $0.3(BaTi_{1-x}Ce_xO_3)$ ceramics [x=0,0.01,0.03,0.05,0.07].

Table 3. Parameters (E_c, P_r, E_s, P_s and W_{rec}) from Electrical hysteresis loops of $0.7BiFeO_3$-$0.3(BaTi_{1-x}Ce_xO_3)$ ceramics [x=0,0.01,0.03,0.05,0.07].

Doping concentration	E_c(kV/Cm^3) x10^3	P_r(μC/Cm^2)	E_s(kV/Cm^3) x10^3	P_s(μC/Cm^2)	W_{rec}(J/cm^3) x10^3
0.00	1.6732	0.030	11.625	0.1955	0.961
0.01	1.0396	0.017	11.070	0.1786	0.894
0.03	1.3567	0.023	11.107	0.1923	0.940
0.05	1.1125	0.016	14.954	0.2298	1.599
0.07	0.7385	0.0092	16.707	0.2331	1.872

4. Conclusions

Ce-doped BF-BT ceramic samples were prepared using a solid-state reaction. The XRD data analysis using the Rietveld refinement program confirmed the formation of a rhombohedral structure with small distortions at room temperature. The obtained Fe-O band angles and bond lengths from the XRD refinement indicated that the Ce ion addition in the BF-BT system influenced the magnetic super-exchange interactions within the FeO_6 octahedral, modifying the ferroelectric and magnetic responses. The FESEM studies revealed that good microstructure with well-defined grain boundaries. The observed variations in Ms and Hc in the magnetic studies support the addition of Ce, which modifies Fe^{3+}-O^{2-}—Fe^{3+} super-exchange interactions, reducing long-range magnetic ordering.

The decrease in the magnetic anisotropy constant at higher Ce concentrations was due to lattice distortions and weak exchange interactions. The observed peak broadening of the dielectric constant with increasing Ce concentration indicates a phase transition of the sample. This phase transition is due to the formation of local strain fields due to the difference between the ionic radii of the Ce and Ti ions. The dielectric loss tangent is stable at long-range temperatures. The observed thin P-E loops indicate a shift from ferroelectric relaxor behavior due to structural disorder and weaker domain-wall pinning.

The energy storage density improved with the addition of Ce ions, indicating that the samples retained ferroelectric energy storage potential. The enhanced efficiency of the samples at higher concentrations indicated that these materials are suitable for actuator applications.

References

[1] N. A. Spaldin, Proc. R. Soc. A Math. Phys. Eng. Sci. **476**, 20190542 (2020); https://doi.org/10.1098/rspa.2019.0542
[2] R. A. M. Gotardo, D. S. F. Viana, M. Olzon-Dionysio, S. D. Souza, D. Garcia, J. A. Eiras, M. F. S. Alves, L. F. Cótica, I. A. Santos, A. A. Coelho, J. Appl. Phys. **112**, (2012); https://doi.org/10.1063/1.4766450
[3] D. Lebeugle, D. Colson, A. Forget, M. Viret, A. M. Bataille, A. Gukasov, Phys. Rev. Lett. **100**, (2008); https://doi.org/10.1103/physrevlett.100.227602
[4] S. Kharbanda, N. Dhanda, A.-C. A. Sun, A. Thakur, P. Thakur, J. Magn. Magn. Mater. **572**, 170569 (2023); https://doi.org/10.1016/j.jmmm.2023.170569
[5] M. S. Bernardo, Bol. Soc. Esp. Ceram. Vidrio **53**, 1–14 (2014); https://doi.org/10.3989/cyv.12014
[6] M. Yao, L. Cheng, S. Hao, S. Salmanov, M. Otonicar, F. Mazaleyrat, B. Dkhil, Appl. Phys. Lett. **122**, (2023); https://doi.org/10.1063/5.0139017
[7] N. Itoh, T. Shimura, W. Sakamoto, T. Yogo, Ferroelectrics **356**, 19–23 (2007); https://doi.org/10.1080/00150190701508860
[8] Mst. S. Mostari, N. Islam, Md. A. Matin, Ceram. Int. **46**, 15840–15850 (2020); https://doi.org/10.1016/j.ceramint.2020.03.131
[9] S. O. Leontsev, R. E. Eitel, J. Am. Ceram. Soc. **92**, 2957–2961 (2009); https://doi.org/10.1111/j.1551-2916.2009.03313.x
[10] H. Singh, A. Kumar, K. L. Yadav, Mater. Sci. Eng. B **176**, 540–547 (2011); https://doi.org/10.1016/j.mseb.2011.01.010
[11] M. H. Lee, D. J. Kim, J. S. Park, S. W. Kim, T. K. Song, M. Kim, W. Kim, D. Do, I. Jeong, Adv. Mater. **27**, 6976–6982 (2015); https://doi.org/10.1002/adma.201502424
[12] S. Cheng, B.-P. Zhang, L. Zhao, K.-K. Wang, J. Mater. Chem. C **6**, 3982–3989 (2018); https://doi.org/10.1039/c8tc00329g
[13] J. Rout, R. N. P. Choudhary, Phys. Lett. A **380**, 288–292 (2015); https://doi.org/10.1016/j.physleta.2015.10.007
[14] J. W. Liang, X. L. Zhu, L. Zhu, L. Liu, S. Y. Wu, X. Q. Liu, X. M. Chen, J. Alloys Compd. **901**, 163681 (2022); https://doi.org/10.1016/j.jallcom.2022.163681
[15] I. Calisir, A. A. Amirov, A. K. Kleppe, D. A. Hall, J. Mater. Chem. A **6**, 5378–5397 (2018); https://doi.org/10.1039/c7ta09497c
[16] D. Wang, A. Khesro, S. Murakami, A. Feteira, Q. Zhao, I. M. Reaney, J. Eur. Ceram. Soc. **37**, 1857–1860 (2016); https://doi.org/10.1016/j.jeurceramsoc.2016.10.027
[17] R. Rai, I. Bdikin, M. A. Valente, A. L. Kholkin, Mater. Chem. Phys. **119**, 539–545 (2009); https://doi.org/10.1016/j.matchemphys.2009.10.011
[18] S. Hajra, V. Vivekananthan, M. Sahu, G. Khandelwal, N. P. M. J. Raj, S.-J. Kim, Nano Energy **85**, 105964 (2021); https://doi.org/10.1016/j.nanoen.2021.105964
[19] H. Dai, F. Ye, Z. Chen, T. Li, D. Liu, J. Alloys Compd. **734**, 60–65 (2017); https://doi.org/10.1016/j.jallcom.2017.11.012
[20] B. S. Kar, M. N. Goswami, P. C. Jana, P. S. Das, J. Mater. Sci. Mater. Electron. **30**, 2154–2165 (2018); https://doi.org/10.1007/s10854-018-0487-x
[21] H. Singh, K. L. Yadav, Ceram. Int. **41**, 9285–9295 (2015); https://doi.org/10.1016/j.ceramint.2015.03.212
[22] K. Momma, F. Izumi, J. Appl. Crystallogr. **44**, 1272–1276 (2011); https://doi.org/10.1107/S0021889811038970
[23] B. S. Kar, M. N. Goswami, P. C. Jana, Integr. Ferroelectr. **213**, 75–92 (2021); https://doi.org/10.1080/10584587.2020.1859826

[24] J. Sharma, B. H. Bhat, A. Kumar, S. Kumar, T. Kaur, B. Want, A. K. Srivastava, Mater. Res. Express **4**, 036104 (2017); https://doi.org/10.1088/2053-1591/aa6433
[25] D. Padalia, U. C. Johri, M. G. H. Zaidi, Mater. Chem. Phys. **169**, 89–95 (2015); https://doi.org/10.1016/j.matchemphys.2015.11.034
[26] L. P. Curecheriu, M. Deluca, Z. V. Mocanu, M. V. Pop, V. Nica, N. Horchidan, M. T. Buscaglia, V. Buscaglia, M. Van Bael, A. Hardy, L. Mitoseriu, Phase Transit. **86**, 703–714 (2013); https://doi.org/10.1080/01411594.2012.726730
[27] D. Makovec, Z. Samardžija, D. Kolar, J. Solid State Chem. **123**, 30–38 (1996); https://doi.org/10.1006/jssc.1996.0148
[28] M. Shang, P. Ren, Y. Wan, X. Lu, J. Eur. Ceram. Soc. **43**, 2488–2497 (2023); https://doi.org/10.1016/j.jeurceramsoc.2023.01.033
[29] S. Liu, L. Zhang, J. Wang, Y. Zhao, X. Wang, Ceram. Int. **43**, 10683–10690 (2017); https://doi.org/10.1016/j.ceramint.2017.04.164
[30] L. Ben, D. C. Sinclair, Appl. Phys. Lett. **98**, (2011); https://doi.org/10.1063/1.3563710
[31] W. Li, X. He, Y. Liu, O. V'yunov, D. Pang, ACS Appl. Electron. Mater. **5**, 6974–6984 (2023); https://doi.org/10.1021/acsaelm.3c01361
[32] Z. Chen, X. Bu, B. Ruan, J. Du, P. Zheng, L. Li, F. Wen, W. Bai, W. Wu, L. Zheng, Y. Zhang, J. Eur. Ceram. Soc. **40**, 5450–5457 (2020); https://doi.org/10.1016/j.jeurceramsoc.2020.06.073